Visualization of a hexagonal boron nitride monolayer on an ultra-thin gold film via reflected light microscopy

Hattori, Yoshiaki
Taniguchi, Takashi
Watanabe, Kenji
Kitamura, Masatoshi

(Citation)
Nanotechnology,33(6):065702

(Issue Date)
2022-02-05

(Resource Type)
journal article

(Version)
Accepted Manuscript

Visualization of a hexagonal boron nitride monolayer on an ultra-thin gold film via reflected light microscopy

Received xxxxxx
Accepted for publication xxxxxx
Published xxxxxx

Abstract

Hexagonal boron nitride (h-BN) is an important insulating layered material for two-dimensional heterostructure devices. Among many applications, few-layer h-BN films have been employed as superior tunneling barrier films. However, it is difficult to construct a heterostructure with ultra-thin h-BN owing to the poor visibility of flakes on substrates, especially on a metallic surface substrate. Since reflectance from a metallic surface is generally high, a h-BN film on a metallic surface does not largely influence reflection spectra. In the present study, a thin Au layer with a thickness of ~10 nm deposited on a Si substrate with a thermally grown SiO_2 was used for visualizing h-BN flakes. The thin Au layer possesses conductivity and transparency. Thus, the $Au/SiO_2/Si$ structure serves as an electrode and contributes to the visualization of an ultra-thin film according to optical interference. As a demonstration, the wavelength-dependent contrast of exfoliated few-layer h-BN flakes on the substrate was investigated under a quasi-monochromatic light using an optical microscope. A monolayer h-BN film was recognized in the image taken by a standard digital camera using a narrow band-pass filter of 490 nm, providing maximum contrast. Since the contrast increases linearly with the number of layers, the appropriate number of layers is identified from the contrast. Furthermore, the insulating property of a h-BN flake is examined using a conductive atomic force microscope to confirm whether the thin Au layer serves as an electrode. The tunneling current through the h-BN flake is consistent with the number of layers estimated from the contrast.

Keywords: h-BN, 2D materials, insulating film, optical interferometry, C-AFM

1. Introduction

Hexagonal boron nitride (h-BN) is an important insulating layered material for two-dimensional (2D) heterostructure devices. This is because h-BN has a potential that it reduces charge scattering and provides an ideal interface for other 2D materials. Therefore, a h-BN film with a thickness of several nanometers has been used as a gate insulator in field-effect transistors [1]. Furthermore, a few-layer h-BN film has been also employed as a tunneling barrier film for the following applications: field-effect transistors with low contact resistance [2, 3], resonant tunneling diodes [4, 5], light-emitting devices [6], and memory devices [7, 8].

As a technique to find exfoliated few-layer h-BN flakes on a substrate, Si substrates with a thermally-grown SiO_2 layer with a thickness of ~90 or ~300 nm have been used to enhance the optical contrast of atomically thin flakes of 2D materials according to the interference effect [9]. However, it has been still difficult to clearly observe a monolayer h-BN film, even if this technique would be applied for the purpose. The contrast of monolayer h-BN is a few percentage, which is smaller than that of monolayer graphene or other 2D transition metal dichalcogenides [9–11]. This is caused by the wide bandgap of about ~6 eV [12], resulting in transparency in the visible wavelength range. Meanwhile, a few-layer h-BN film is typically formed on a metallic thin film electrode with a thickness of the order of 10 nm for electronic device applications [2, 3, 7, 13, 14]. In this case, the contrast of the h-BN film decreases further. This is because the high reflectance of the metallic electrode suppresses interference enhancement [15].

Conversely, a properly designed multilayer substrate, including a thin metallic layer as a top layer, enhances the contrast of a thin film placed on the substrate. When a top metallic layer is sufficiently thin, light with a frequency above the plasma frequency of the metallic layer passes through the layer. A Au layer with a thickness of ~10 nm is both

conductive and transparent to light with a wavelength less than ~520 nm. Therefore, a thin Au layer serves as an optically dielectric material with a large extinction index in the wavelength range. The use of a thin Au layer placed on a Si substrate with an ~90-nm-thick SiO_2 layer has enhanced the contrast of a thin film on the Au surface at a wavelength of ~500 nm [16, 17, 18]. Syahir et al. demonstrated the detection of the monolayer of 1-Amino-8-octanethiol with a thickness of a few nanometers adsorbed on Au/poly(methyl methacrylate)/Ag substrate by reflection spectroscopy using an optical fiber [16]. In addition, Hattori et al. identified the number of alkyl-chines of alkanethiol monolayer on a $Au/SiO_2/Si$ substrate by measuring the contrast in an image taken with an optical microscope [17]. Recently, Donnelly et al. have applied a $Au/SiO_2/Si$ substrate to observe a monolayer of MoS_2 [15]. Furthermore, Huang has reported a theoretical model to visualize a monolayer of 2D material using a microscope [11]. Nevertheless, it has been unclear whether a monolayer h-BN formed only on a metallic surface could be experimentally seen using an optical microscope.

In the current study, we investigated whether a monolayer h-BN film on an $Au/SiO_2/Si$ substrate can be directly observed using a standard reflected optical microscope. First, the electrical, optical, and morphological properties of $Au/SiO_2/Si$ substrates without h-BN are demonstrated. Then, the contrast between substrates with and without h-BN films is explained on the basis of theoretical calculations. Exfoliated few-layer h-BN flakes are placed on a substrate; photographs are shown to prove that those are observable. The contrast estimated from these photographs is compared to theoretically calculated contrast. Finally, the insulating property of few-layer h-BN flakes on $Au/SiO_2/Si$ substrates is investigated using a conductive atomic force microscope (C-AFM).

2. Experimental methods

2.1 Preparation

Few-layer h-BN flakes on $Au/SiO_2/Si$ substrates were prepared as follows. Si substrates with a thermally grown 94-nm-thick SiO_2 film were cleaned in deionized water, acetone, and isopropyl alcohol for ~5 min each with an ultrasonic cleaner. Then, the substrates were exposed to UV/ozone for 15 min. An adhesive 0.5-nm-thick Cr layer and an Au film were deposited on the substrates at a rate of ~0.15 Å/s under a pressure of the order of 10^{-4} Pa with a thermal evaporator equipped with a quartz crystal microbalance thickness monitor. Since Au is chemically inert metal in ambient conditions, Au films were used in the study. Although the Cr adhesive layer is used in the layer structure, the $Au/Cr/SiO_2/Si$ structure is simply expressed as $Au/SiO_2/Si$ in the current study. The thickness of the Au layer was in the range of 6–30 nm. For the substrate with a 7-nm-thick Au layer, the surface typically had a root-mean-square roughness of 0.5 nm. The substrate was stored in N_2 (O_2 < 10 ppm, H_2O < 10 ppm) until it was used for the next process. Hexagonal BN single crystals grown at high pressure and temperature [19] were used as materials for the following method. Hexagonal BN flakes on a substrate were prepared by a mechanical exfoliation technique and transfer method from the h-BN single crystal.

2.2 Characterization

Thin h-BN flakes were identified using an optical microscope (LV150; Nikon, Japan) equipped with either a monochrome 12-bit camera (CS-63M; Bitran, Japan) cooled down to 10°C or a color 8-bit camera (EOS Kiss X4; Canon, Japan). Objective lenses of 50× with a numerical aperture (NA) of 0.8 (LU Plan 50×; Nikon) and 150× with a NA of 0.90 (LU Plan Apo 150×; Nikon) were used for monochromatic and color images, respectively. A narrow band-pass filter was inserted in the optical path only after the collector lens of the halogen lamp in the microscope. The full width at half maximum (FWHM) of the narrow band-pass filters is 10 nm. To obtain superior images, the aperture stop was closed so that the entire light disk size in the eye tube is ~80%. This corresponds to a substantial reduction in NA. An ellipsometer (Auto SE; Horiba, Japan), a fiber-optic spectrophotometer (Film Tek 1000; SCI, USA) with a spot size of ~5 mm, and a scanning electron microscope (SEM) (FE-SEM, S-5000; Hitachi, Japan) with an accelerating voltage of 10 kV were used for measuring SiO_2 film thickness and reflection spectra and observing the surface, respectively.

Morphological and electrical investigations were performed with an AFM (NanoNavi; SII, Japan) in the contact mode at room temperature in ambient air (50% relative humidity, ~20°C). A Si cantilever (SI-DF3-R, SII Nano-Technology, Japan) with a nominal curvature of 30–50 nm and stiffness of 1.6 N/m was used. For electrical measurement, a 25-nm-thick, adhesive Cr layer and a 50-nm-thick Au layer were deposited on the AFM tip by thermal evaporation at a rate of ~1.0 Å/s after UV/ozone treatment. In the C-AFM measurement, the Au substrate is electrically connected to a semiconductor device parameter analyzer (B1500A; Keysight Technology, USA) by a copper wire with a drying silver paste (D-500; Fujikura Kasei, Japan). The parasitic resistance, including the resistance of thin Au film and silver paste and the contact resistance of the AFM tip, is <100 Ω, which is less than the resistance of h-BN flakes. The maximum output current was limited to 1 mA to avoid a breakdown [20, 21]. In the measurement, the resistance of the tunneling barrier film is measured. Generally, conductivity through an AFM tip decreases when a metal layer coated on the AFM tip peels off by mechanical scanning. When the parasitic resistance of >100 Ω is observed for an AFM tip, we redeposited Au/Cr layers on the AFM tip. Typically, the AFM tips used in the current study were coated up to three times. The radius

curvature of the AFM tip is estimated to be ~100 nm from the SEM observations in **Fig. S1** in Supplementary Infomation. Regarding current variation in the electrical measurement, the roughness of the Au film induces the difference in the contact condition between an AFM tip and a h-BN surface [22], causing a primary variation. The variation is small compared to the position dependence of a h-BN flake and/or difference in an AFM tip. Thus, the dependence of the resistance on AFM tips is probably small in the study.

2.1 Calculation of optical contrast

The visibility of h-BN films is attributed to the difference in reflectance ($R = |r|^2$) between the substrate on which the film is placed and the substrate on which the film is not placed. Here, r represents the complex reflectivity. The optical contrast (C) is quantitatively evaluated by ($R_{BN}/R_{sub} - 1$). The subscripts, BN and sub, denote the h-BN film and bare substrate, respectively. The bare substrate means a substrate on which no h-BN film is placed. r for the multilayer substrate can be numerically calculated using the transfer matrix method [11, 23, 24]. In the optical model, the refractive index of h-BN is set to 2.2 [25]. The refractive index of 0.5-nm-thick Cr film is set to $2.0 - 0.5i$ as a chromium oxide [26], where i is an imaginary unit. In general, Cr films easily oxidize. In the present study, it is possible that the ultra-thin Cr film oxidizes by bonding with oxygen in the residual gas of the vacuum and/or by being in contact with the underlying SiO_2 layer. The refractive index of chromium oxide effectively reproduces experimental reflectance. Since the influence of dopants in the Si substrate on the refractive index is small in the visible wavelength region [27], it was excluded in the calculation. The digital integer value D of each pixel in an image reflects the R value. Thus, experimental C values are simply defined from the image as $C = D_{BN}/D_{sub} - 1$. The incident and reflected light onto the substrate contains light tilted from the surface normal by an angle (θ_0) equal to one-half of the objective angular aperture defined by $\sin\theta_0 = \mathrm{NA}$. In addition, experimental C contains the effect on the wavelength width of a narrow band-pass filter. Thus, the effect should be included in the numerical calculation for credible comparison. As the average value of R, the total reflectivity intensity ($\bar{R}$) for a narrow band-pass filter with a central wavelength of λ' and an FWHM of λ_{FWHM} is given by

$$\bar{R}(\lambda') = \frac{1}{(\tan\theta_0)^2 \lambda_{FWHM}} \int_{\lambda'-\lambda_{FWHM}/2}^{\lambda'+\lambda_{FWHM}/2} \int_0^{\theta_0} \left(|r_p(\lambda,\theta)|^2 + |r_s(\lambda,\theta)|^2 \right) \tan\theta (\sec\theta)^2 d\theta d\lambda \quad (1)$$

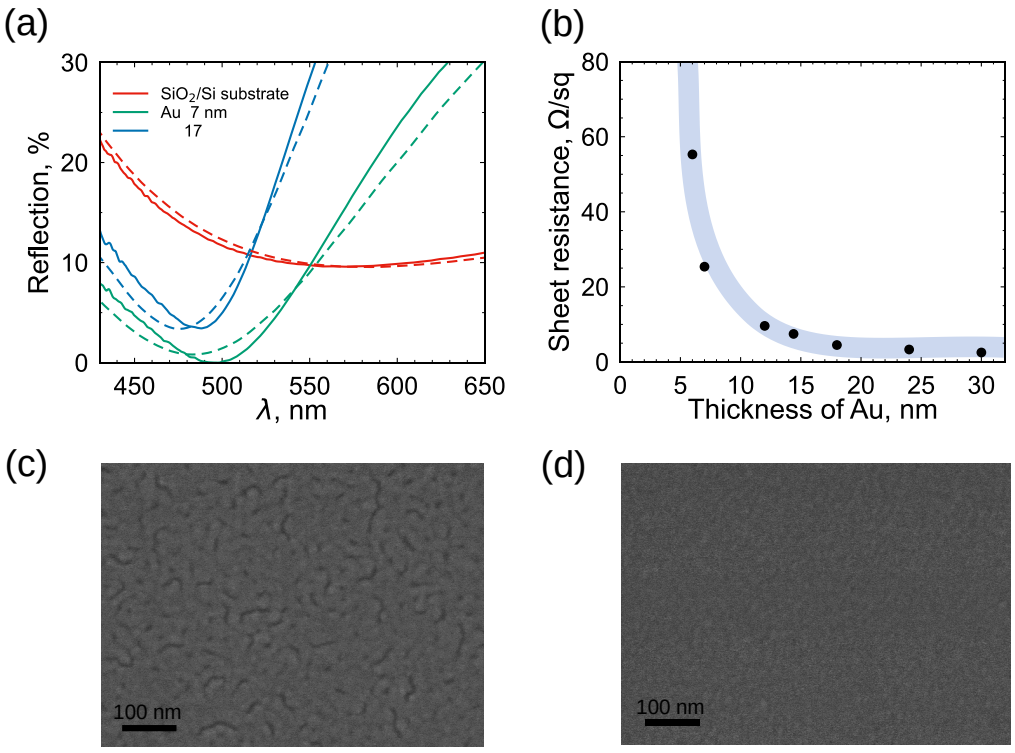

Figure 1. Optical, electrical, and morphological characteristics of Au/SiO_2/Si substrates without h-BN films. **(a)** Reflection spectroscopy of Au/SiO_2/Si and SiO_2/Si substrates. The solid and broken lines represent the experiment and calculation results, respectively. **(b)** Sheet resistance as a function of Au thickness. The light blue line represents a guide for the eyes. **(c)**, **(d)** SEM image of Au film with a thickness of 7 and 12 nm, respectively.

as a double integral of angle (θ) and wavelength (λ) [17, 28, 29]. Here, $r_p(\lambda, \theta)$ and $r_s(\lambda, \theta)$ are oblique reflectivities for *p* and *s* components of light, respectively. Then, the wavelength-dependent *C* is calculated by $(\bar{R}_{\mathrm{BN}}/\bar{R}_{\mathrm{sub}} - 1)$

2. Results and discussion

Figure 1(a) shows the experimental and theoretical reflection spectra. The experimental spectra were obtained using a fiber-optic spectrophotometer. The red, blue, and green solid lines represent the experimental spectra for the SiO_2/Si substrate with no Au layer, an 17-nm-thick Au layer, and a 7-nm-thick Au layer, respectively. In all spectra, reflection decreases with λ below a certain λ and increases above λ. Thus, the spectrum has the minimum reflection at the λ value. For the SiO_2/Si substrate with no Au layer, the spectrum exhibits a minimum reflection of 10% at ~580 nm. For the SiO_2/Si substrate with an Au layer, the spectrum exhibits a minimum reflection at ~500 nm. The reflection is 5% for the 17-nm-thick Au layer and close to 0% for the 7-nm-thick Au layer. The dashed lines represent the theoretical spectra, corresponding to the experimental ones, and are used to calculate the optical model of multilayer structures shown in **Fig. 2(a)**. The theoretical spectra roughly reproduce the experimental spectra and exhibit a minimum reflection at a specific λ. Although the visibility of a thin film placed on a substrate depends on both reflections from the substrate with and without the thin film [11, 17], R_{sub} can predict the contrast and wavelength at which the contrast is maximum. The SiO_2/Si substrate exhibits the minimum reflection of 10% at 580 nm, as shown in **Fig. 1(a)**. Thus, it is expected that the visibility of a thin film on the substrate would be the maximum around the λ. This expectation is consistent with a study on the observation of a monolayer h-BN on a SiO_2/Si substrate [10]. On the other hand, the Au/SiO_2/Si substrate has the minimum reflection at λ = ~500 nm, which is lower than the SiO_2/Si substrate. Because the sensitivity of the ultra-thin film increases as reflectance decreases, it is expected that the thin Au film contributes to the enhancement of the visibility of a thin film. The enhancement has been confirmed experimentally and theoretically [15– 17].

Figure 1(b) shows the experimental sheet resistance of SiO_2/Si substrates with Au layers with different thicknesses obtained using Van der Pauw's method [30]. Thickness dependence is useful to discuss the applicability of the substrate as a conductive substrate. The substrate with a 5-nm-thick Au layer had a sheet resistance of many orders of magnitude larger than 55 Ω/sq for a 6-nm-thick Au layer and is regarded as non-conductive. The light blue line represents a guide for the eyes. Resistance decreases with an increase in thickness. The substrate with 6- and 7-nm-thick Au layers has

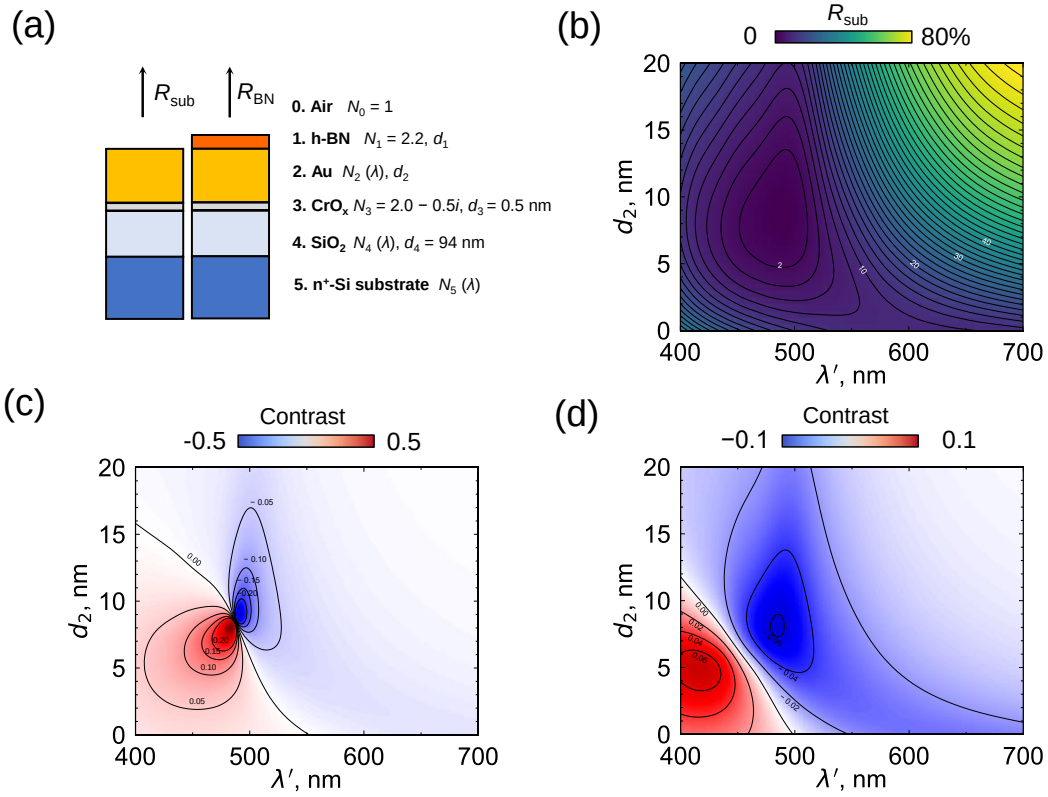

Figure 2. Simulation of reflection and contrast of the substrate. **(a)** Calculation model. **(b)** Reflection spectra of Au/SiO_2/Si substrate for NA = 0.0. **(c)**, **(d)** Contour map of the contrast of monolayer h-BN as a function of the thickness of Au and λ' for NA = 0.3 and NA = 0.8, respectively.

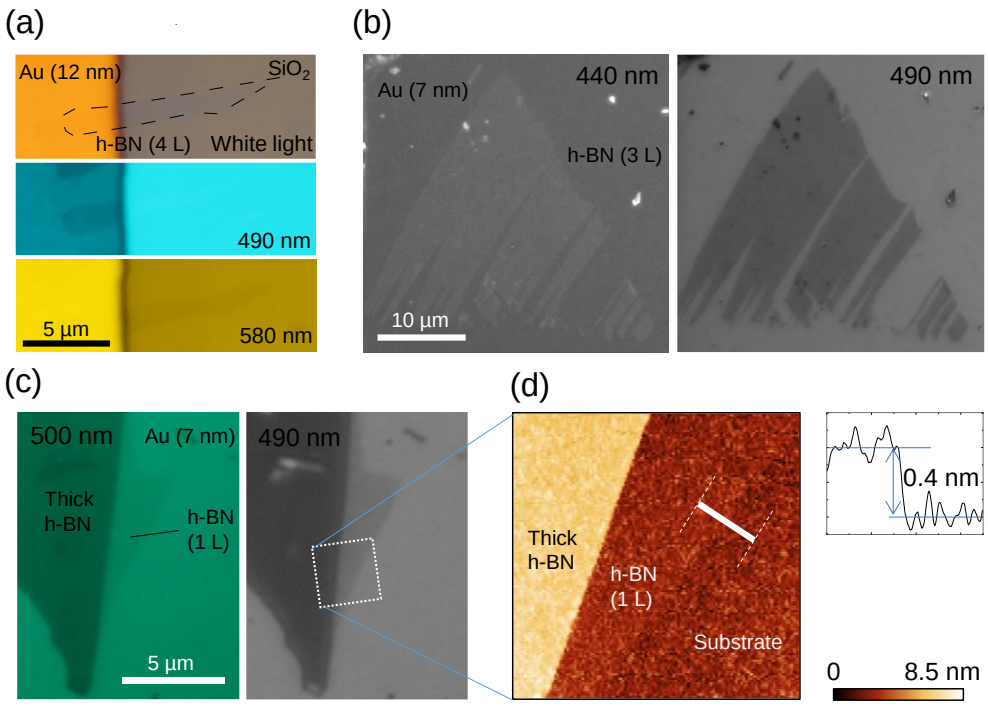

Figure 3. Optical microscopic image of few-layer h-BN films. All color and monochrome images are taken by the objective of 150× with NA = 0.9 and 50× with NA = 0.8, respectively. All color images are raw data without image processing. **(a)** Color image of 4-L h-BN partly placed on Au/SiO_2/Si substrate. The top photo is for white light illumination. The middle and bottom photos are for λ' = 490 nm and λ' = 580 nm, respectively. **(b)** Monochrome photo of 3 L h-BN. The left and right photos are for λ' = 440 nm and λ' = 490 nm, respectively. **(c)** Photo of 1-L h-BN. The left is the image obtained by the color camera for λ' = 500; the right is the monochrome image for λ' = 490 nm. **(d)** Height AFM image for the dotted region in **(c)**. The right graph presents the average height profile for the white solid line in the AFM image, indicating 1-L h-BN.

a sheet resistance of ~55 and 25 Ω/sq, respectively. The substrate with an Au layer of thickness of 7 nm or more could be available for electrical measurement. The morphological observation of Au layers supports the explanation of electrical conductivity. **Figures 1(c) and 1(d)** show the SEM images for 7- and 12-nm-thick Au layers, respectively. The 7-nm-thick Au layer appears to have a percolation pattern. [31, 32]. In the SEM image of **Fig. 1(c)**, dark areas representing island discontinuities are observed. Probably, such a discontinuity area increases the sheet resistance.

Before showing the results of the observation of thin h-BN films on an Au layer, contrast is verified by calculations. **Figure 2(b)** represents a contour map of reflection (R_{sub}) for Au/SiO_2/Si substrates shown in **Fig. 2(a)**. The reflection was calculated as a function of Au thickness (d_2) and λ' for NA = 0, which corresponds to the calculation of **Fig. 1(a)**. The contour map shows that R_{sub} has a minimum value around d_2 = 9 nm and λ' = 500 nm. From the expectation described in the first paragraph of this section, the calculation result suggests that a substrate with a 9-nm-thick Au layer on SiO_2/Si substrate provides a large contrast at λ = ~500 nm. Notably, through observations by an optical microscope, the oblique light passing through the high NA objective decreases visibility [11, 24]. In the present study, this decrease is quantitatively examined as follows.

Figures 2(c) and 2(d) show the contrast calculated for a monolayer (1 L) h-BN film on an Au substrate assuming NA = 0.3 and NA = 0.8, respectively. The NA values of 0.3 and 0.8 correspond to those of a standard objective lens with 10× and 50×, respectively. For both NA cases, the contrast has positive and negative peaks. The dependence of contrast frequently appears in the observation of thin 2D materials on SiO_2/Si substrates with no Au layer [10]. For NA = 0.3, the positive and negative peaks appear at d_2 = 8 nm and λ' = 480 nm and d_2 = 9 nm and λ' = 490 nm, respectively. The value of d_2 and λ' is close to that for the minimum reflection of the substrate without a h-BN film. The closeness is predicted above. On the other hand, for NA = 0.8, both positive and negative peaks shift to small d_2 and short λ'. Especially, the shift of the positive peak is large. This suggests that the microscopic observation using a high NA lens leads to a large shift of d_2 and λ' values of high contrast from those of the minimum reflection. Another point is that the d_2 value of the negative peak is larger than that of the positive peak. This aspect is important when using an Au substrate for electrical measurement. A substrate with a thick Au layer is desired for

electrical measurement. This is because a thin Au layer increases electrical resistance. The visibility of a thin layer on an Au substrate is governed by the absolute value of contrast, regardless of whether the contrast is positive or negative. Thus, negative contrast is more suitable than positive contrast when an Au substrate is used for electrical measurement. The contrast in **Figs. 2(c) and 2(d)** was calculated for a h-BN layer of 1 L on an Au substrate. The contrast calculated for a h-BN layer of 2 and 4 L is shown in **Figs. S2(a)** and **S2(b)**, respectively. The dependence of the contrast for multilayer is similar to that for 1 L. In particular, the d_2 and λ' values of positive and negative peaks are almost the same for 1 L and a multilayer.

Next, the visibility of h-BN flakes formed on an Au substrate is experimentally examined. Few-layer h-BN flakes were selected on the substrate by the color camera with an appropriate filter. **Figure 3(a)** shows the color photographs taken for a h-BN flake of four layers (L) on a SiO_2/Si substrate partially covered with an Au (12 nm)/Cr (0.5 nm) layer, which was deposited through a metal mask. The left and right sides are Au and SiO_2 surfaces, respectively. The top photograph was taken under white light illumination. The dashed black line represents the area of the h-BN flake. It is difficult to recognize h-BN flakes, especially the part on the Au surface. The middle (bottom) photograph was taken when light passed through a narrow band-pass filter of $\lambda' = 490$ (580) nm, which provides the highest contrast for a flake on a substrate with (without) an Au layer. The area of the h-BN flake is seen on the Au surface for $\lambda' = 490$ nm and on the SiO_2 surface for $\lambda' = 580$ nm. Compared with the middle and bottom photographs, the area of the h-BN flake on the Au surface for $\lambda' = 490$ nm is more obvious than that on the SiO_2 surface for $\lambda' = 580$ nm. The high contrast on the Au surface is attributed to the low reflection. Note that all color photographs in **Fig. 3** are depicted from raw data, which were not processed on any software.

The use of a monochrome camera provides a good agreement between the experimental and theoretical contrasts. **Figure 3(b)** shows the photos of 3-L h-BN flakes on a 7-nm-thick Au film for $\lambda' = 440$ nm (left) and 490 nm (right). The reflection from the area covered with the h-BN flake is higher than that from the uncovered area for $\lambda' = 440$ nm. Meanwhile, the reflection from the area covered with the h-BN flake is lower than that from the uncovered area for $\lambda' = 490$ nm. The high and low reflections correspond to the positive and negative contrasts obtained by calculation, respectively. **Figure 3(c)** shows a 1-L h-BN flake on a 7-nm-thick Au film for the color and monochrome camera. **Figure 3(d)** shows a height AFM image corresponding to the area surrounded by the dotted line shown in **Fig. 3(c)**. The inset on the right is the height profile along the white solid line in the height AFM image. The height at a point on the solid line is the average of the height values on the line passing through the point, perpendicular to the solid line, and has thelength of two dashed lines. The height step of 0.4 nm indicates a monolayer flake [10, 33]. Certainly, 1-L h-BN films on an Au layer can be optically observed using a standard reflected optical microscope equipped with a digital camera.

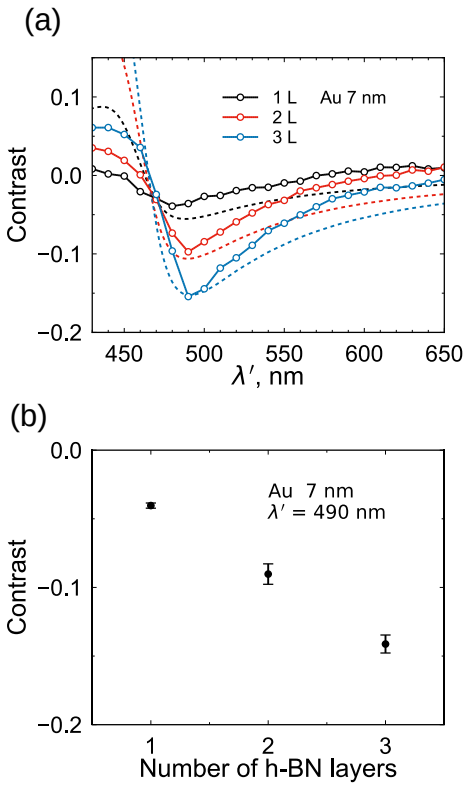

Figure 4. Contrast of 1–3-L h-BN on a 7-nm Au film. The contrast is obtained by the monochrome images taken by the objective of 50× with NA = 0.8. **(a)** Contrast as a function of λ with simulation. The open circles and broken lines represent the experiment and calculation, respectively. **(b)** Contrast at $\lambda' = 490$ nm. The plots and error bars indicate the average and standard deviation, respectively. The number of samples for 1 L, 2 L, and 3 L is 6, 4, and 3, respectively.

The contrast is qualitatively evaluated by the monochrome camera with 50× objective lens (NA = 0.8). **Figure 4(a)** shows the contrast spectra of 1–3-L h-BN films on a 7-nm Au layer. The solid and dashed lines represent the experimental and theoretical contrast spectra. For all numbers of layers, the contrast has a negative peak at λ' of ~490 nm. **Figure 4(b)** shows the contrast at $\lambda' = 490$ nm. The contrast increases with an increase in the number of layers. Therefore, the number of layers can be simply identified from the contrast estimated from an image taken using a narrow band-pass filter. Note that the contrast of 0.04 for 1 L is ~1.5 times as large as that on the optimized Si/SiO_2 substrate [10]. θ_0 in Eq. (1) was used as a fitting parameter to calculate the theoretical contrast in **Fig.**

4(a). This is because the aperture stop was closed down, and the substantial NA (= sin θ_0) was less than that of the objective. When the substantial NA equals 0.75, the theoretical contrast spectra closely match the experimental contrast spectra.

Next, the insulating property of a h-BN flake is discussed regarding the current–voltage (*I*–*V*) characteristics. Few-layer h-BN flakes are examined using a C-AFM with a Au-coated cantilever after optically determining the number of layers. **Figure 5(a)** shows a simplified illustration of the measurement setup. The *I*–*V* curves measured for 1–3-L h-BN films are shown in **Fig. 5(b)**. No electrical defects, such as pinholes, were observed in the measurement. For all numbers of layers, the *I*–*V* curve was nearly antisymmetric. This is because both electrodes are composed of Au. As described below, electrodes providing different barrier heights (φ_B) lead to an anti-asymmetry curve. In addition, the current increases linearly with *V* at low voltages, as indicated by the dashed line, and nonlinearly increases with *V* at high voltages. The linear relation is attributed to the direct tunneling current, which is dominated in the low voltage regime [25, 26]. The tunneling current is given by

$$I(V) = \frac{A_{eff}\sqrt{m\phi_B}q^2V}{h^2 d_1} exp\left(\frac{-4\pi\sqrt{m\phi_B}d_1}{h}\right), \quad (2)$$

where A_{eff}, m, q, and h represent the effective contact area, free electron mass, elementary charge, and Plank's constant, respectively. **Equation (2)** explains the linear increase in the tunneling current. **Figure 5(c)** shows the resistance estimated from the *I*–*V* curves at low voltages for 1–3-L h-BN films. The resistance exponentially increases with an increase in the number of layers. This behavior is explained by **Eq. (2)**. This is because d_1 in the exponent rather than d_1 in the denominator is dominant in $I(V)$. Accordingly, unknown parameters, A_{eff} and φ_B, can be estimated by fitting a line to experimental data. The details are described in **Fig. S3**. The A_{eff} and φ_B values were estimated to be 5.0 (±1.5) × 10^2 nm^2 and φ_B = 1.7 (±0.4) eV by a least-squares method, respectively. The resistance calculated from **Eq. (2)** using these parameters is shown as a solid red line in **Fig. 5(c)**. The extracted A_{eff} is equivalent to a circular area with a 25-mm diameter, which corresponds to the contact area between the AFM tip and the surface of h-BN. The contact area is reasonable from the shape of the AFM tip shown in **Fig. S1**. The obtained φ_B value is the barrier height to hole carriers, which is the difference between the valence band maximum of h-BN and the Fermi energy of Au [34], and it is comparable to those reported in previous studies [22, 34, 35].

The nonlinear increase at high voltages is attributed to Fowler–Nordheim (FN) tunneling, which is expressed by

$$I(V) = \frac{A_{eff}q^3mV^2}{8\pi h\phi_B m^* d_1^2} exp\left(\frac{-8\pi\sqrt{2m^*}\phi_B^{\frac{3}{2}}d_1}{3hqV}\right) \quad (3)$$

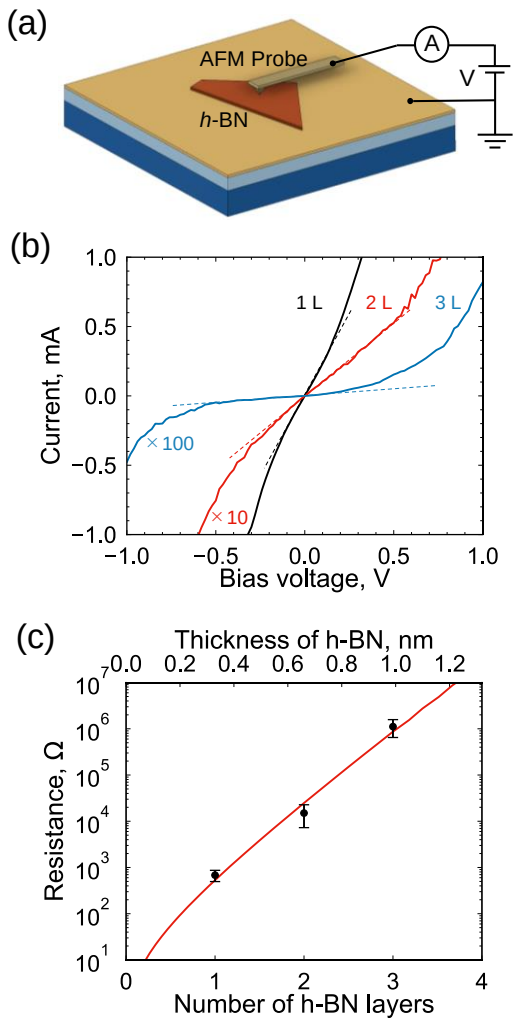

Figure 5. Conductive-AFM measurement. **(a)** Schematic of the system. **(b)** *I*–*V* curves for 1–3 layers, indicating hole tunneling current. **(c)** Resistance of direct tunneling. The red lines represent the theoretical value for A_{eff} = 5.0 (±1.5) × 10^2 nm^2 and φ_B = 1.7 (±0.4) eV. The plots and error bars indicate the average and standard deviation, respectively. The number of samples for 1 L, 2 L, and 3 L is 27, 23, and 13, respectively.

where m^* represents the hole effective mass. The exponent in **Eq. (3)** contains *V*. Thus, *I* nonlinearly increases with *V*. FN tunneling is dominant in h-BN films with four or more layers. **Equation (3)** is useful for extracting A_{eff} and φ_B by FN plots [35] or line fitting [22, 34]. However, it does necessitate further investigation, which the current study does not provide. This is because the obtained *I*–*V* curve transits from direct tunneling to FN tunneling. As the summary of the C-AFM measurement, it was confirmed that the thinnest h-BN flake optically found on the substrate is electrically a monolayer and it certainly retains insulating properties on the Au substrate. In other words, a practical electrical measurement can be

conducted while observing the monolayer of h-BN on an Au layer.

In the present study, we focus on h-BN flakes placed on a Si substrate with a 94-nm-thick SiO_2 layer. A SiO_2 layer with a thickness of ~90 nm has frequently been used for observing a thin film on the surface. However, the thickness has not been optimized as a substrate with a conductive layer such as an Au layer. A thick Au layer is required for the fabrication process controllability, low resistance, mechanical stability, and flatness of the layer. Meanwhile, a thick Au film decreases the visibility. Therefore, it is necessary to determine the thickness of an Au film according to an ultra-thin film to achieve the requirement. Although there is a mismatch in the contrast for 1-L h-BN between the experiment and calculation, let us consider optimization using **Fig. 2(c, d)**. If one can obtain a large 1-L h-BN flake, the film can be observed by a low NA objective. Since the current experimental setup could detect the contrast of at least 0.04, the film on a 17-nm-thick Au layer might be recognized with a NA = 0.3 objective at $\lambda' = 500$ nm, as shown in **Fig. 2(c)**. Au thickness is the optimized value for the 1-L h-BN on a Si substrate with a 94-nm-thick SiO_2 layer in the setup. However, the optimized thickness of Au also depends on the thickness of the SiO_2 film. Therefore, by optimizing the thickness of the SiO_2 film, the thickness of the Au film can be increased. From this viewpoint, a 115-nm-thick SiO_2 layer rather than a 94-nm-thick SiO_2 layer might be suitable for visualizing a thin film on the surface. The contrast calculated for the SiO_2 film with a thickness of 115 and 150 nm that corresponds to **Fig. 2(c, d)** is shown in **Fig. S4**, respectively. It is expected that a 16-nm-thick Au film on a 115-nm SiO_2 film might visualize the exfoliated 1-L h-BN with a NA = 0.8 objective at $\lambda' = 510$ nm in the standard setup. As discussed above, to visualize an ultra-thin film, it is important to determine Au thickness appropriately while considering the characteristics of an ultra-thin film (refractive index, thickness, and size) and the measurement system (magnification of the objective, NA value, stop aperture, sensitivity of the camera, and FWHM of optical filter).

Conclusions

A Au layer with a thickness of ~10 nm deposited on a SiO_2 (94 nm)/Si substrate with a 0.5-nm-thick Cr adhesive layer exhibited semi-transparency and electrical conductivity. The experimental reflection from the Au substrate, depending on λ, was close to 0% at λ = ~500 nm. An ultra-thin film formed on the Au surface changed reflection spectra. The change provided contrast between the ultra-thin film and the Au surface. As a result, the ultra-thin film formed on the Au surface, with electrical conductivity, is visible in the image taken using an optical microscope.

As a demonstration, the exfoliated few-layer h-BN flakes on the substrate were observed under a quasi-monochromatic light using an optical microscope. The wavelength-dependent contrast roughly agrees with that calculated from a multilayer model. The monolayer h-BN is visible in the image taken with a commercial digital color camera with a narrow band-pass filter of 490 nm. Since the contrast increases linearly with the number of layers, the appropriate number of layers can be identified optically. In addition, the insulating properties of few-layer h-BN flakes were investigated using a C-AFM, which was electrically connected to a semiconductor device parameter analyzer. The insulating properties extracted from the electrical measurement were comparable to those reported in earlier works. Despite practical concerns regarding an adhesive layer, a non-flat surface, and oblique incident light, it has been confirmed that the use of a Au/Cr/SiO_2/Si substrate is valid for detecting a few-layer h-BN flake formed on the substrate.

References

[1] Dean C R, Young A F, Meric I, Lee C, Wang L, Sorgenfrei S, Watanabe K, Taniguchi T, Kim P and Shepard K L 2010 Boron nitride substrates for high-quality graphene electronics *Nature nanotechnology* **5** 722–6

[2] Wang J, Yao Q, Huang C-W, Zou X, Liao L, Chen S, Fan Z, Zhang K, Wu W and Xiao X 2016 High Mobility MoS_2 transistor with low Schottky barrier contact by using atomic thick h-BN as a tunneling layer *Advanced materials* **28** 8302–8

[3] Cui X, Shih E-M, Jauregui L A, Chae S H, Kim Y D, Li B, Seo D, Pistunova K, Yin J and Park J-H 2017 Low-temperature ohmic contact to monolayer MoS_2 by van der Waals bonded Co/h-BN electrodes *Nano letters* **17** 4781–6

[4] Gaskell J, Eaves L, Novoselov K S, Mishchenko A, Geim A K, Fromhold T M and Greenaway M T 2015 Graphene-hexagonal boron nitride resonant tunneling diodes as high-frequency oscillators *Applied Physics Letters* **107** 103105

[5] Mishchenko A, Tu J S, Cao Y, Gorbachev R V, Wallbank J R, Greenaway M T, Morozov V E, Morozov S V, Zhu M J and Wong S L 2014 Twist-controlled resonant tunnelling in graphene/boron nitride/graphene heterostructures *Nature nanotechnology* **9** 808–13

[6] Withers F, Del Pozo-Zamudio O, Schwarz S, Dufferwiel S, Walker P M, Godde T, Rooney A P, Gholinia A, Woods C R and Blake P 2015 WSe_2 light-emitting tunneling transistors with enhanced brightness at room temperature *Nano letters* **15** 8223–8

[7] Wu X, Ge R, Chen P-A, Chou H, Zhang Z, Zhang Y, Banerjee S, Chiang M-H, Lee J C and Akinwande D 2019 Thinnest nonvolatile memory based on monolayer h-BN *Advanced Materials* **31** 1806790

[8] Li D, Wang X, Zhang Q, Zou L, Xu X and Zhang Z 2015 Nonvolatile floating-gate memories based on stacked black phosphorus–boron nitride–MoS_2 heterostructures *Advanced Functional Materials* **25** 7360–5

[9] Gorbachev R V, Riaz I, Nair R R, Jalil R, Britnell L, Belle B D, Hill E W, Novoselov K S, Watanabe K and Taniguchi T 2011 Hunting for monolayer boron nitride: optical and Raman signatures *Small* **7** 465–8

[10] Blake P, Hill E W, Castro Neto A H, Novoselov K S, Jiang D, Yang R, Booth T J and Geim A K 2007 Making graphene visible *Applied physics letters* **91** 063124
[11] Gorbachev R V, Riaz I, Nair R R, Jalil R, Britnell L, Belle B D, Hill E W, Novoselov K S, Watanabe K and Taniguchi T 2011 Hunting for monolayer boron nitride: optical and Raman signatures *Small* **7** 465–8
[12] Huang F 2019 Optical contrast of atomically thin films *The Journal of Physical Chemistry C* **123** 7440–6
[13] Cassabois G, Valvin P and Gil B 2016 Hexagonal boron nitride is an indirect bandgap semiconductor *Nature photonics* **10** 262–6
[14]Chandni U, Watanabe K, Taniguchi T and Eisenstein J P 2015 Evidence for defect-mediated tunneling in hexagonal boron nitride-based junctions *Nano letters* **15** 7329–33
[15]Donnelly G E, Velickỳ M, Hendren W R, Bowman R M and Huang F 2020 Achieving extremely high optical contrast of atomically-thin MoS_2 *Nanotechnology* **31** 145706
[16]Syahir A, Mihara H and Kajikawa K 2010 A new optical label-free biosensing platform based on a metal- insulator- metal structure *Langmuir* **26** 6053–7
[17]Hattori Y, Takahashi H, Ikematsu N and Kitamura M 2021 Chain-Length Dependence of Optical Properties for an Alkanethiol Monolayer on an Ultrathin Gold Film Revealed via Reflected Light Microscopy *The Journal of Physical Chemistry C* **125** 14991–9
[18]Velický M, Donnelly G E, Hendren W R, McFarland S, Scullion D, DeBenedetti W J, Correa G C, Han Y, Wain A J and Hines M A 2018 Mechanism of gold-assisted exfoliation of centimeter-sized transition-metal dichalcogenide monolayers *ACS nano* **12** 10463–72
[19]Watanabe K, Taniguchi T and Kanda H 2004 Direct-bandgap properties and evidence for ultraviolet lasing of hexagonal boron nitride single crystal *Nature materials* **3** 404–9
[20]Hattori Y, Taniguchi T, Watanabe K and Nagashio K 2015 Layer-by-layer dielectric breakdown of hexagonal boron nitride *ACS nano* **9** 916–21
[21]Cui Z, He Y, Tian H, Khanaki A, Xu L, Shi W and Liu J 2020 Study of Direct Tunneling and Dielectric Breakdown in Molecular Beam Epitaxial Hexagonal Boron Nitride Monolayers Using Metal–Insulator–Metal Devices *ACS Applied Electronic Materials* **2** 747–55
[22]Britnell L, Gorbachev R V, Jalil R, Belle B D, Schedin F, Katsnelson M I, Eaves L, Morozov S V, Mayorov A S and Peres N M 2012 Electron tunneling through ultrathin boron nitride crystalline barriers *Nano letters* **12** 1707–10
[23]Yoon D, Moon H, Son Y-W, Choi J S, Park B H, Cha Y H, Kim Y D and Cheong H 2009 Interference effect on Raman spectrum of graphene on SiO_2/Si *Physical Review B* **80** 125422
[24]Casiraghi C, Hartschuh A, Lidorikis E, Qian H, Harutyunyan H, Gokus T, Novoselov K S and Ferrari A C 2007 Rayleigh imaging of graphene and graphene layers *Nano letters* **7** 2711–7
[25]Ohba N, Miwa K, Nagasako N and Fukumoto A 2001 First-principles study on structural, dielectric, and dynamical properties for three BN polytypes *Physical Review B* **63** 115207
[26]Ivanova T, Gesheva K, Cziraki A, Szekeres A and Vlaikova E 2008 Structural transformations and their relation to the optoelectronic properties of chromium oxide thin films *Journal of Physics: Conference Series* vol **113** (IOP Publishing) p 012030
[27]Barta E 1977 Determination of effective mass values by a Kramers-Kronig analysis for variously doped silicon crystals *Infrared Physics* **17** 111–9
[28]Katzen J M, Velický M, Huang Y, Drakeley S, Hendren W, Bowman R M, Cai Q, Chen Y, Li L H and Huang F 2018 Rigorous and accurate contrast spectroscopy for ultimate thickness determination of micrometer-sized graphene on gold and molecular sensing *ACS applied materials & interfaces* **10** 22520–8
[29]Lu Y, Li X-L, Zhang X, Wu J-B and Tan P-H 2015 Optical contrast determination of the thickness of SiO_2 film on Si substrate partially covered by two-dimensional crystal flakes *Science Bulletin* **60** 806–11
[30]van der Pauw L J 1958 A method of measuring specific resistivity and Hall effect of discs of arbitrary shape *Philips Res. Rep.* **13** 1–9
[31]Doron-Mor I, Barkay Z, Filip-Granit N, Vaskevich A and Rubinstein I 2004 Ultrathin Gold Island Films on Silanized Glass. Morphology and Optical Properties *Chem. Mater.* **16** 3476–83
[32]Wanunu M, Vaskevich A and Rubinstein I 2004 Widely-Applicable Gold Substrate for the Study of Ultrathin Overlayers *J. Am. Chem. Soc.* **126** 5569–76
[33]Li L H, Cervenka J, Watanabe K, Taniguchi T and Chen Y 2014 Strong Oxidation Resistance of Atomically Thin Boron Nitride Nanosheets *ACS Nano* **8** 1457–62
[34]Hattori Y, Taniguchi T, Watanabe K and Nagashio K 2018 Determination of Carrier Polarity in Fowler–Nordheim Tunneling and Evidence of Fermi Level Pinning at the Hexagonal Boron Nitride/Metal Interface *ACS Appl. Mater. Interfaces* **10** 11732–8
[35]Lee G-H, Yu Y-J, Lee C, Dean C, Shepard K L, Kim P and Hone J 2011 Electron tunneling through atomically flat and ultrathin hexagonal boron nitride *Appl. Phys. Lett.* **99** 243114

Supplementary Information for:

Visualization of a hexagonal boron nitride monolayer on an ultra-thin gold film via reflected light microscopy

Yoshiaki Hattori[1, *], Takashi Taniguchi[2], Kenji Watanabe[3], and Masatoshi Kitamura[1, *]

[1] Department of Electrical and Electronic Engineering, Kobe University, 1-1, Rokkodai-cho, Nada, Kobe, 657-8501, Japan

[2] International Center for Materials Nanoarchitectonics,

National Institute for Materials Science, 1-1 Namiki, Tsukuba 305-0044, Japan

[3] Research Center for Functional Materials,

National Institute for Materials Science, 1-1 Namiki, Tsukuba 305-0044, Japan

Corresponding authors:

Email: hattori@eedept.kobe-u.ac.jp, kitamura@eedept.kobe-u.ac.jp

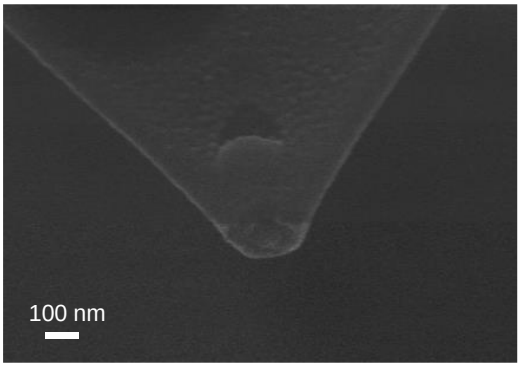

Figure S1. The SEM image of the AFM tip after electrical measurement with an accelerating voltage of 10 kV.

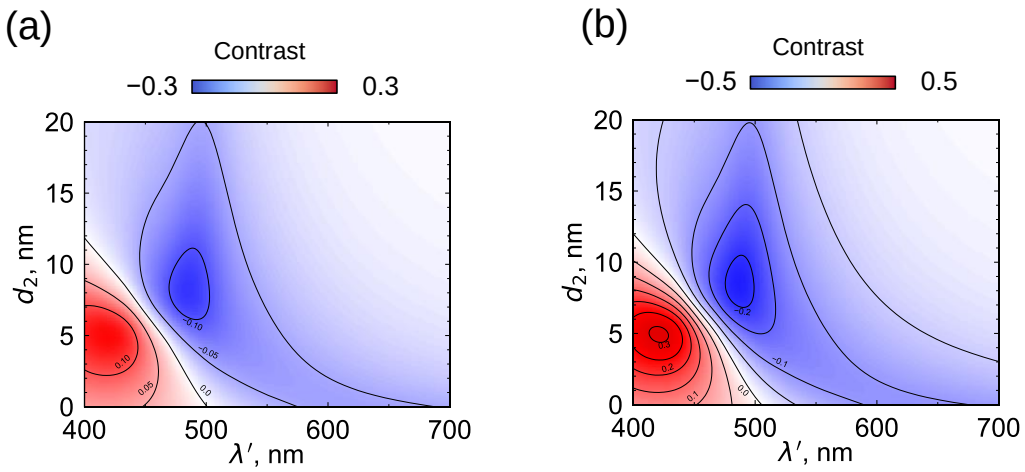

Figure S2. Simulation of contour map of the contrast of 2-L **(a)** and 4-L **(b)** h-BN on the Au/SiO_2/Si substrate for a 94-nm SiO_2 film and NA = 0.8 as a function of the thickness of Au and λ', which is comparable to **Fig. 2(d)**.

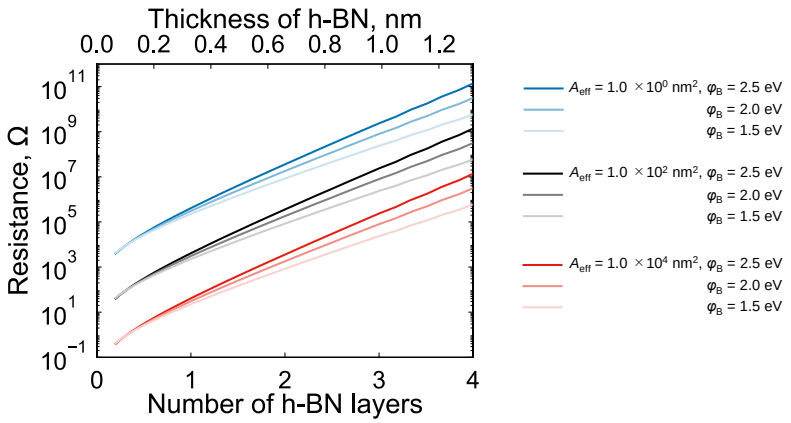

Figure S3. Theoretical resistance of the direct tunneling with different A_{eff} and φ_B.

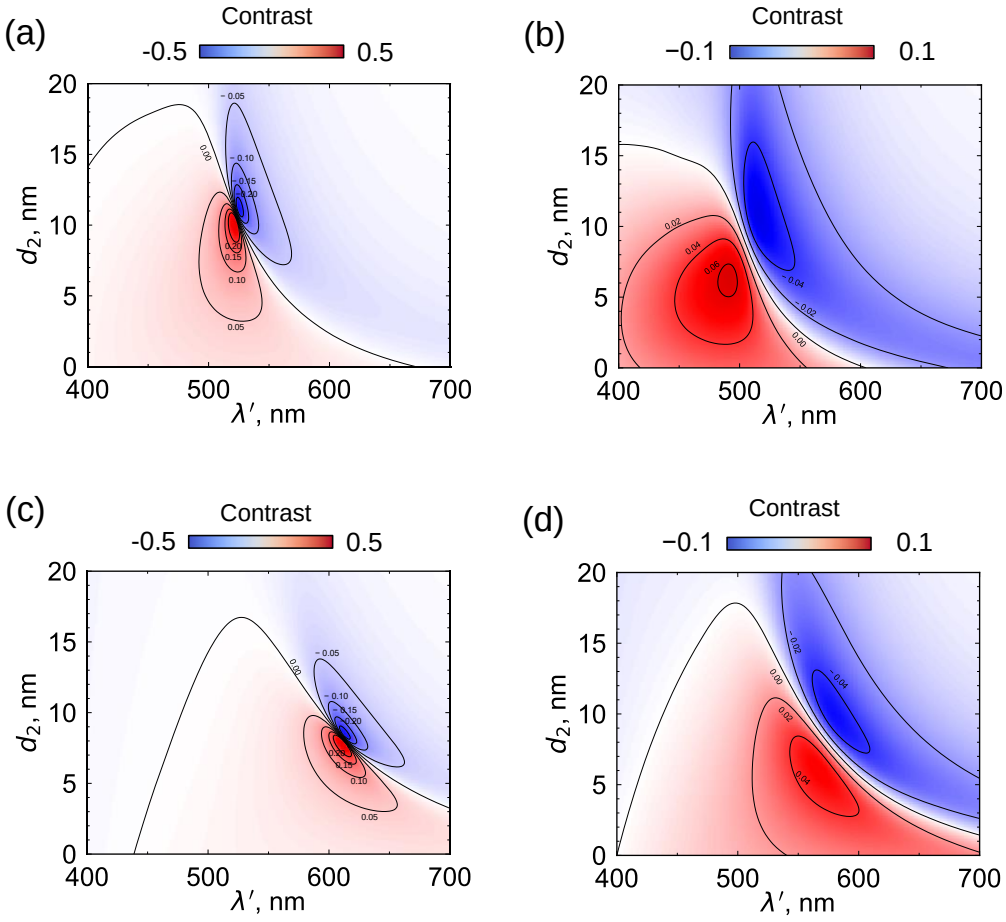

Figure S4. Simulation of contour map of the contrast of monolayer h-BN on the substrate for 115- and 150-nm SiO_2 films as a function of the thickness of Au and λ, which is comparable to **Fig. 2(c, d)**. **(a)** 115-nm SiO_2 of NA = 0.3. **(b)** 115-nm SiO_2 of NA = 0.8. **(c)** 150-nm SiO_2 of NA = 0.3. **(d)** 150-nm SiO_2 of NA = 0.8.